PHARMACEUTICAL BIOLOGY
2026, VOL. 64, NO. 1, 1222–1244
https://doi.org/10.1080/13880209.2026.2761697

Taylor & Francis
by informa

RESEARCH ARTICLE

OPEN ACCESS Check for updates

γ-Cyclodextrin enhances the biopharmaceutical performance of *Boswellia serrata* extract: comparative *in vitro* and *ex vivo* evaluation

Marcell Stifter-Mursits[a,b*], Péter Püski[c*], Vivien Bárdos[a,b], Barbara Ádám[a,b], Levente Szőcs[a,b], Dávid Hamar[d,b], Nikolett Kállai-Szabó[d,b], István Antal[d,b], Judit Hohmann[c,e], Attila Hunyadi[c,e], Fang-Rong Chang[f], Bence Sipos[g], Gábor Katona[g], Réka Angi[a,b] and György T. Balogh[a,b,h]

[a]Department of Pharmaceutical Chemistry, Semmelweis University, Budapest, Hungary; [b]Center for Pharmacology and Drug Research & Development, Semmelweis University, Budapest, Hungary; [c]Institute of Pharmacognosy, University of Szeged, Szeged, Hungary; [d]Department of Pharmaceutics, Semmelweis University, Budapest, Hungary; [e]HUN-REN–USZ Biologically Active Natural Products Research Group, University of Szeged, Szeged, Hungary; [f]Graduate Institute of Natural Products, Kaohsiung Medical University, Kaohsiung, Taiwan; [g]Institute of Pharmaceutical Technology and Regulatory Affairs, University of Szeged, Szeged, Hungary; [h]Department of Chemical and Environmental Process Engineering, Faculty of Chemical Technology and Biotechnology, Budapest University of Technology and Economics, Budapest, Hungary

ABSTRACT

Context: Poor oral bioavailability of boswellic acids (BAs) restricts the therapeutic potential of *Boswellia serrata* extracts (BSE), primarily due to low solubility and limited intestinal absorption.

Objective: This study systematically evaluated cyclodextrin (CD)-based BSE formulations to identify a composition with the potential to enhance the biopharmaceutical performance of BAs.

Materials and methods: Native and substituted CDs were screened for BA solubilization. Selected BSE formulations were prepared by lyophilization and physical mixing and characterized using HPLC, FT-IR, PXRD and DSC. Dissolution was evaluated in fasted- and fed-state biorelevant media, followed by intestinal parallel artificial membrane permeability assay (PAMPA) and *ex vivo* porcine intestinal permeation studies.

Results: The greatest solubility enhancements were provided by γ-CDs. Lyophilizates markedly enhanced BA dissolution, with approximately 8–10-fold higher release in fasted-state medium and complete release in fed-state medium. In PAMPA, HP-γ-CD increased apparent BA permeability by up to 3–5-fold in fasted-state medium, versus 1.7–2.8-fold for native γ-CD. Conversely, *ex vivo* studies identified native γ-CD as the superior carrier, increasing cumulative BA permeation approximately 15-fold.

Discussion: The superior performance of γ-CDs is consistent with the hypothesis that their larger cavity provides favorable accommodation of bulky BAs. The contrasting PAMPA and *ex vivo* outcomes indicate that biopharmaceutical performance depends on the balance between solubilization, free-drug availability and membrane interactions rather than solubilization capacity alone.

Conclusion: Native γ-CD demonstrated the most favorable overall performance, particularly in the *ex vivo* permeation model, supporting further evaluation of its potential to improve intestinal absorption of BAs.

ARTICLE HISTORY

Received 14 September 2026
Revised 2 November 2026
Accepted 5 November 2026

KEYWORDS

Boswellia serrata extract; boswellic acids; γ-cyclodextrin inclusion complex; *in vitro* dissolution; *ex vivo* intestinal permeation

CONTACT György T. Balogh balogh.gyorgy.tibor@semmelweis.hu; Réka Angi angi.erzsebet@semmelweis.hu Department of Pharmaceutical Chemistry, Semmelweis University, Budapest, Hungary
*Co-first authors and contributed equally to this work.

Supplemental data for this article can be accessed online at https://doi.org/10.1080/13880209.2026.2761697.

© 2026 The Author(s). Published by Informa UK Limited, trading as Taylor & Francis Group.
This is an Open Access article distributed under the terms of the Creative Commons Attribution License (http://creativecommons.org/licenses/by/4.0/), which permits unrestricted use, distribution, and reproduction in any medium, provided the original work is properly cited. The terms on which this article has been published allow the posting of the Accepted Manuscript in a repository by the author(s) or with their consent.

Introduction

From religious ceremonies to evidence-based science and therapy

Boswellia serrata Roxb. ex Colebr. (Burseraceae) is a small- to medium-sized tree or shrub native to arid and semi-arid regions of India. When its bark is incised, it exudes an oleo-gum-resin referred to as frankincense (Al-Harrasi et al. 2019). Historical documentation indicates that the use of frankincense originates from antiquity. It was burned as incense in religious ceremonies, funeral pyres, and secular celebrations. Frankincense became a symbol of worship of God, kings, and rulers. At the birth of Jesus, the three Eastern kings brought gifts of gold, frankincense, and myrrh to honor the infant. Various types of frankincense have been used to ward off evil spirits, unpleasant odors, and to facilitate meditation (Thulin 2020).

In addition to its religious and cultural importance, frankincense has historically been valued as a traditional remedy in Ayurvedic, Traditional Chinese Medicine, Unani, and Western medicine (Siddiqui 2011). Since the early 2000s, clinical trials have evaluated frankincense preparations for various inflammatory and immune-related disorders, including osteoarthritis (Kimmatkar et al. 2003), inflammatory bowel disease (Madisch et al. 2007), while mainly preclinical evidence indicates potential anticancer activity (Efferth and Oesch 2022). Meanwhile, dietary supplements derived from frankincense extract have become widely used for alleviating symptoms of arthritis and inflammatory bowel disease (Introspective Market Research 2024).

Pharmacokinetic limitations of boswellic acids

Despite their widespread use, the plasma concentrations of orally administered boswellic acids (BAs), the major bioactive constituents of *B. serrata*, remain low relative to several proposed pharmacological targets (Abdel-Tawab et al. 2011). Suboptimal systemic exposure is primarily attributed to the low aqueous solubility of BAs, which limits gastrointestinal dissolution and intestinal absorption, thereby restricting effective inhibition of targets such as microsomal prostaglandin E_2 synthase-1 (mPGES-1) and cathepsin G (Tausch et al. 2009; Siemoneit et al. 2011). In addition to dissolution-limited intestinal absorption, systemic exposure is further reduced by first-pass metabolism and enterocyte accumulation (Krüger et al. 2008; Gerbeth et al. 2013). Strong binding of BAs to serum albumin further affects their free plasma fraction, distribution and pharmacological availability (Siemoneit et al. 2009). Distribution of BAs is influenced by their very high lipophilicity, with compounds such as β-boswellic acid (βBA) showing enhanced accumulation in lipid-rich tissues, including the brain (Reising et al. 2005).

Food intake markedly alters the pharmacokinetic profile of *B. serrata* extracts (BSE). Co-administration of BSE with a high-fat meal has been reported to increase systemic exposure to BAs by 3–6 times (Sterk et al. 2004). This effect is likely mediated by bile salt-induced micellar solubilization, which enhances the dissolution and intestinal absorption of these highly lipophilic compounds (Solanki et al. 2024). However, formulation strategies are crucial for enhancing solubility, absorption, and to reduce variability of oral delivery.

Formulation strategies for boswellic acids

Several formulation strategies have been explored to enhance the solubility, absorption and systemic exposure of BAs. Some representative formulation approaches are summarized in Table 1. Phospholipid-based systems, such as Casperome™ and BSE naturosomes, micellar formulations such as Sol-BE, and polymeric systems such as 3-*O*-acetyl-11-keto-β-boswellic acid (AKBA)-loaded poly(lactic-co-glycolic acid) (PLGA) nanoparticles have demonstrated improved solubility, systemic exposure and pharmacological effects in preclinical and clinical settings. However, the results of Schmiech et al. (2024) also highlight the complexity of translating increased systemic exposure into improved therapeutic efficacy, as enhanced bioavailability did not yield proportionally stronger anti-inflammatory effects.

Table 1. Formulation strategies for enhancing the bioavailability of boswellic acids (Cyclodextrin-based strategies are highlighted with a grey background).

Formulation / API / excipient	Models / conditions	Main outcomes	Reference
Aflapin® AKBA-enriched BSE combined with nonvolatile oil fractions of the oleo-gum-resin	*In vitro:* human chondrocytes and synovial cells *In vivo:* oral administration in Sprague–Dawley rats in a Complete Freund's Adjuvant (CFA)-induced inflammation model	*In vitro:* ↑ glycosaminoglycan production; ↓ IL-1β-induced chondrocyte death; ↑ MMP-3 inhibition *In vivo:* ↑ AKBA exposure (AUC ↑~50% compared to 5-Loxin®); ↑ anti-inflammatory efficacy in the CFA-model	Sengupta et al. 2011
Phospholipid-based BSE complex combined with nonionic polymeric surfactant Pluronic® F127 (1:1:1, w/w/w)	*In vitro*: Caco-2 permeability model *In vivo*: oral administration in rats (240 mg/kg)	*In vitro:* ↑ BAs solubility ×54; ↑ permeability; ↑ net flux *In vivo*: ↑ KBA ×26; ↑ AKBA ×14; ↑ AKBA brain ×5	Hüsch et al. 2012
Casperome™ (Phytosome®) BSE combined with soy lecithin at 1:1 (w/w)	*In vivo*: oral administration in female Wistar rats (240 mg/kg BSE)	*In vivo*: ↑ KBA ×7 (AUC); ↑ β-BA ×3 (AUC); ↑ brain KBA/AKBA ×35 and β-BA ×3; ↑ distribution to poorly vascularized tissues such as the eye (up to ×17)	Hüsch et al. 2013
AKBA encapsulated in PLGAnanoparticles (PLGA/AKBA 50:10) using polyvinyl alcohol and trehalose	*In vitro*: dialysis bag diffusion *In vivo*: oral administration in female Sprague–Dawley rats; (50 mg/kg); evaluated in a carrageenan-induced paw edema model	*In vitro*: biphasic release profile with ~61% drug release over 72 h *In vivo*: ↑ AUC ×9; ↑ C_{max} ×6; ↑ $t_1/_2$ ×2.1; ↑ paw edema inhibition (67% vs 41%)	Bairwa and Jachak 2015
Sol-BE BSE solubilized using AQUANOVA micellar technology	*In vivo*: oral administration in female albino Wistar rats (128 mg/kg)	*In vivo:* ↑ AKBA ×56 (AUC); ↑ C_{max} ×25; KBA detected only with formulation; ↑ other BAs up to ×5 (AUC); ↔ T_{max} (6–8 h)	Meins et al. 2018
BA:Poloxamer complexes (P188 and P407)	*In vitro*: solubility and dissolution studies using physical mixtures, kneading and solvent evaporation methods (pH 1.2 and 6.8)	*In vitro*: ↑ solubility; ↑ drug release; most effective systems were P188 (1:2) and P407 (1:1) prepared by kneading	Tambe and Pandita 2018
BSE naturosomes phospholipid-based nanonised BSE prepared with hydrogenated soy phosphatidylcholine (phospholipid:BSE 3.5:1 w/w)	*In vitro* solubility and dissolution *Ex vivo*: intestinal permeation using everted rat intestine *In vivo* CFA-induced arthritis model in male Wistar rats (oral, 180 mg/kg)	*In vitro*: ↑ solubility ×16; dissolution >99% (vs ~31% non-formulated BSE) *Ex vivo*: ↑ intestinal permeation (20→79%, 3 h) *In vivo*: ↑ anti-inflammatory efficacy; ↓ paw thickness/ volume; ↓ TNF-α; ↓ cartilage & bone degradation	Usapkar et al. 2024
Boswellia-Loges® Micellar *Boswellia serrata* extract with polysorbate 20 vs Biotikon® BS-85 non-formulated native extract in HPMC capsules	*In vitro*: reporter Jurkat JE6.1 lymphocytes transfected with an NF-κB reporter vector *Ex vivo*: whole blood collected 2 and 5 h after administration and stimulated with lipopolysaccharide *In vivo*: single-dose, open-label, crossover study in healthy volunteers (oral, 800 mg, fed state)	*In vitro*: similar NF-κB inhibition, with slightly stronger reduction of TNF-α release for the native extract *Ex vivo* ↓ TNF-α, IL-6 & IL-8 (both formulations); no superiority of micellar formulation; ↓ IL-1β for the native extract *In vivo*: ↑ Cmax ×2–5; ↑ AUC ×2–6; ↑ relative bioavailability (AKBA ×43); ↓ Tmax; no superior anti-inflammatory efficacy	Schmiech et al. 2024
AβBA and AKBA γ-CD complexes	*In vitro*: androgen-independent PC-3 prostate cancer cells *In vivo*: PC-3 xenograft models in the chick chorioallantoic membrane and nude mice; topical and systemic administration of the AKBA–γ cyclodextrin complex	*In vitro*: AβBA and AKBA inhibited NF-κB signaling *via* IKK inhibition; induced apoptosis, associated with decreased B-cell lymphoma (Bcl-2, Bcl-xL) and cyclin D1 expression; AKBA showed stronger activity than AβBA; *In vivo*: ↓ tumor growth; induce apoptosis (dose-dependent); no systemic toxicity	Syrovets et al. 2005
AKBA-γ-CD complexes	*In vivo*: psoriasis ($CD18^{hypo}$) model in mice; intraperitoneal injection daily for 21 or 35 days	*In vivo*: peak plasma concentration 100 µM; rapid elimination; ↓ NF-κB; ↓ TNF-α, MCP-1, IL-12 & IL-23 (dose-dependent)	Wang et al. 2009

(*Continued*)

Table 1. Continued.

Formulation / API / excipient	Models / conditions	Main outcomes	Reference
Unspecified BSE–CD complex	*In vivo*: Schistosoma japonicum egg-induced liver granuloma model in mice; treatment during granuloma formation	*In vivo*: ↓ Liver granuloma; ↓ ALT, AST, LTB4, PGE2 & MMP-9 (mRNA/protein); ↔ worm burden & egg load	Liu et al. 2013
AKBA: β-CD and HP-β-CD complexes	*In vitro*: Physicochemical characterization, phase solubility and dissolution studies with molecular modeling (pH 1.2 and 6.8)	*In vitro*: A_N-type phase solubility (stability constants of 380.2 M^{-1} for β-CD and 145.9 M^{-1} for HP-β-CD); enhanced dissolution compared to the free BAs; AKBA:CD 1:2 ratio showed superior performance	Tambe et al. 2018
AKBA: HP-β-CD:Poloxamer ternary dispersions	*Ex vivo*: everted gut sac model using rat jejunum	*Ex vivo*: ↑ AKBA permeability ×17	Tambe et al. 2019

Despite these advances, alternative formulation approaches remain essential to optimize the oral performance of BAs. Cyclodextrin-based formulations represent a well-established and clinically validated strategy, with numerous approved drug products utilizing native and modified CDs (Puskás et al. 2023). In this context, CD complexation offers a promising means to improve the pharmacokinetic properties of BAs and potentially enhance their therapeutic performance.

Cyclodextrin-based formulation strategies

Cyclodextrins are cyclic oligosaccharides composed of six, seven or eight α-(1,4)- linked glucopyranose units called alpha-, beta- and gamma-CDs (α-CD, β-CD and γ-CD), respectively (Szejtli 1988). Cyclodextrins can form inclusion complexes with lipophilic compounds in aqueous media, thereby enhancing solubility, permeability, and stability of the guest molecule, ultimately improving bioavailability (Loftsson and Brewster 2012). However, careful selection and optimization of CD type and concentration are crucial, as excessive amount of CD may also hinder membrane partitioning and absorption (Másson et al. 1999; Loftsson and Brewster 2011).

Despite their widespread pharmaceutical use, few studies have examined CD-based systems for BSE or isolated BAs. Earlier studies reported that AKBA–γ-CD complexes inhibited tumor growth and induced apoptosis *in vivo* without observable systemic toxicity (Syrovets et al. 2005). A non-specified BSE–CD formulation reduced the size of liver granuloma and decreased the expression of inflammatory mediators, including leukotriene B4 and prostaglandin E2 (Liu et al. 2013). Encapsulation of 11-keto-β-boswellic acid (KBA) and AKBA with β-CD and HP-β-CD produced inclusion complexes with enhanced solubility and dissolution, as confirmed by phase-solubility studies and solid-state characterization (Tambe et al. 2018). These complexes exhibit markedly improved drug release. In addition, *ex vivo* intestinal absorption studies using the everted gut sac model demonstrated that HP-β-CD complexes and poloxamer-based solid dispersions (SDs) increased the apparent permeability of AKBA compared to the native extract (Tambe and Pandita 2018; Tambe et al. 2019). These findings underscore the potential of CD-based formulations in overcoming the poor solubility and limited intestinal absorption of BAs.

Despite the numerous individual reports, a comprehensive and systematic comparison of CD-based formulations for BSE is still lacking. In particular, the influence of CD cavity size and substitution type on the solubilization and biopharmaceutical behavior of the BAs remains insufficiently characterized. Furthermore, previous studies have predominantly focused on β-CDs in accordance with general formulation trends (Puskás et al. 2023), with limited attention to γ-CDs.

We hypothesized that systematic comparison of CD systems would enable the identification of the most suitable carrier for BAs, with γ-CDs potentially providing advantages for these bulky triterpenoids owing to their larger cavity size. To test this hypothesis, various CD systems were progressively

evaluated and narrowed based on their solubilization, biorelevant dissolution and membrane permeation performance using complementary *in vitro* and *ex vivo* models.

The key novelty of the present study lies in the stepwise evaluation of a broad range of CD-based BSE formulations, progressively narrowing the candidates based on complementary biopharmaceutical criteria. Importantly, the investigation was extended to six major BAs rather than focusing solely on the pharmacopeial marker compounds KBA and AKBA (United States Pharmacopeia 2019; European Directorate for the Quality of Medicines and HealthCare 2023). Ultimately, this approach may contribute to overcoming the key limitations of BAs and facilitate the development of CD-enabled formulations with improved oral bioavailability.

Materials and methods

Materials

The CDs were obtained from CycloLab Ltd. (Budapest, Hungary): α-CD (CY-1001), β-CD (CY-2001), γ-CD (CY-3001), hydroxypropyl-β-CD (HP-β-CD, degree of substitution DS = 4.5, CY-2005), hydroxypropyl-γ-CD (HP-γ-CD, DS = 4.5, CY-3005), sulfobutylether-β-CD (SBECD, DS = 6.5, CY-2041), randomly methylated β-CD (RAMEB, DS = 12.0, CY-2004), and randomly methylated γ-CD (RAMEG, DS = 12.0, CY-3004).

The oleo-gum-resin of *B. serrata* was purchased from TheWholesalerCo (Noida, Uttar Pradesh, India). The steam-distillation by-product of *Boswellia sacra* Flueck. was kindly provided by Enfleurage, Inc. (New York, NY, USA). Reference product (REF), labeled to contain 65% boswellic acids was purchased from GymBeam s.r.o. (Košice, Slovakia, batch no. B11S0S23).

In the present study, BSE denotes the acidic fraction prepared in-house from *B. serrata* oleo-gum-resin, as described below. The terms native and unformulated BSE refer to this fraction without added CD, whereas REF denotes the separately purchased commercial reference product.

Fasted-state simulated intestinal fluid (FaSSIF-V2, V2FAS) powder and fed-state simulated intestinal fluid (FeSSIF-V2, V2FES) powder and concentrate (V2FESBUF) were purchased from Biorelevant.com Ltd. (London, UK). Porcine small intestine was obtained from a local slaughterhouse, Porció-Ék Kft. (Albertirsa, Hungary).

Methanol (AR grade, 05730-101-340), ethyl acetate (AR grade,02930-101-340) and hydrochloric acid (37%, 08710-101-340) were purchased from Molar Chemicals Ltd. (Budapest, Hungary). Whatman No. 4 filter paper was obtained from Whatman International Ltd. (Maidstone, UK). Formic acid (LC-MS grade, 78573-270) and acetonitrile (LC-MS grade, AAA19862-0F) were purchased from VWR International (Radnor, PA, USA).

MQuant® pH indicator paper (1.10232), Millex-GP polyethersulfone (PES) membrane syringe filters (SLGPR33RS), MultiScreen-IP (MAIPN4510) and MultiScreenHTS-PCF (MSSLBCP10) filter plates, deuterated chloroform (1.03420), L-α-phosphatidylcholine (P7443), cholesterol (C8667), dodecane (297879), hexane (52750), chloroform (319988), phosphate-buffered saline (PBS, P3813) and potassium hydroxide (P1767) were purchased from Merck KGaA (Darmstadt, Germany).

Extraction process of Boswellia serrata

The oleo-gum-resin was cooled to −5 °C and ground. A total of 735 g of the ground material was extracted with 3000 mL of MeOH *via* sonication for 10 min, after which the supernatant was collected. To maximize yield, the extraction was performed in triplicate. The combined supernatants were filtered through Whatman No. 4 filter paper, evaporated to dryness under gradually reduced pressure (~50 mbar) at 40 °C using a rotary evaporator equipped with a B-480 water bath and a V-300 vacuum pump (BÜCHI Labortechnik AG, Flawil, Switzerland), and subsequently lyophilized overnight in a Christ Alpha 1–4 LSCplus freeze dryer (Martin Christ Gefriertrocknungsanlagen GmbH, Osterode am Harz, Germany) at a condenser temperature of −50 °C and a final vacuum of 0.10 mbar, yielding the dried MeOH extract.

To obtain the acidic fraction, 340 g of the MeOH extract was dissolved in 3500 mL of a 2% (w/v) aqueous solution of potassium hydroxide, and then liquid-liquid partitioning was performed using ethyl acetate (3 × 1500 mL). The aqueous phase was acidified to pH 4 using 1 M hydrochloric acid and the pH was monitored using indicator paper. Subsequently, the acidified aqueous phase was extracted with ethyl acetate (3 × 1500 mL). The combined organic phases were evaporated and lyophilized under the same conditions described above, yielding 116 g of the acidic fraction, designated as B. serrata extract (BSE). The extraction procedure is illustrated in the (Supplementary Materials Figure S1).

Isolation of triterpene acids from the steam distillation byproduct of Boswellia sacra oleo-gum-resin

The steam distillation of the oleo-gum-resin produces a nonvolatile solid fraction enriched in high-molecular-weight BAs as a by-product. A targeted isolation procedure was performed on this byproduct to obtain the major triterpene acids for further analytical measurement. The detailed isolation procedure is provided in the (Supplementary Materials Figure S2).

Structure elucidation of isolated boswellic acids

^{1}H NMR spectra of the isolated BAs were recorded on a Bruker Avance DRX 500 spectrometer (Bruker Corporation, Rheinstetten, Germany) operating at 500 MHz in $CDCl_3$. The residual solvent signals of $CDCl_3$ (δ_H 7.26) were used as internal references. Spectral analysis and processing were performed using MestReNova 9.0 software.

HPLC analysis

Chromatographic analysis was performed using an Agilent 1260 Infinity HPLC system (Agilent Technologies, Santa Clara, CA, USA). Separation was achieved using an Agilent ZORBAX SB-C_{18} column (50 × 3.0 mm, particle size 1.8 µm). The column temperature was maintained at 45 °C. The injection volume was set to 5 µL. The mobile phases consisted of eluent A: ultrapure water (PW) (produced by a Direct-Q 3 UV purification system (Millipore, Burlington, MA, USA)) containing 0.1% (v/v) formic acid (FA) and eluent B: acetonitrile (ACN) containing 0.1% (v/v) FA. Gradient elution was applied at a constant flow rate of 1.2 mL/min as shown in Table 2. Detection was performed using a diode array detector (DAD) at 210 and 254 nm. Chromatographic data were acquired and processed using the Agilent ChemStation software. The HPLC analysis was performed using six isolated reference standards: KBA, AKBA, α-boswellic acid (αBA), βBA, 3-*O*-acetyl-α-boswellic acid (AαBA), and 3-*O*-acetyl-β-boswellic acid (AβBA).

Cyclodextrin screening

The effect of CDs on BAs solubility was evaluated by preparing CD solutions in PBS 7.4 buffer at 50 mM concentrations (for β-CD, only 12 mM solution was prepared due to solubility limitation). Thirty milligrams of BSE was introduced into vials and mixed with 3 mL of CD solution. The vials

Table 2. Gradient programme for the separation of BAs in BSE.

Time (min)	Eluent A (%)	Eluent B (%)
0.0-2.0	65	35
2.0-8.5	35	65
8.5-12.0	25	75
12.0-15.0	5	95
15.0-17.0	5	95
17.1-19.0	65	35

Table 3. Component amounts in the formulations, and the measured ΣBA content in % (w/w) expressed as mean ± SD ($n = 3$).

ID	CD Type	Method	CD Amount (Dry)	BSE Amount	Measured ΣBA %
L1	γ-CD	Lyophilization	3.00 g	3.00 g	18.9 ± 0.2
L2	HP-γ-CD		3.00 g	3.00 g	18.7 ± 0.2
L3	HP-β-CD		3.00 g	3.00 g	19.2 ± 0.7
F1	γ-CD	Physical mixture	3.00 g	3.00 g	19.6 ± 0.5
F2	HP-γ-CD		3.00 g	3.00 g	18.8 ± 1.1
F3	HP-β-CD		3.00 g	3.00 g	18.9 ± 0.6
BSE	Native *B. serrata* extract (used to prepare the formulations)				38.6 ± 0.5
REF	Marketed *B. serrata* extract with magnesium stearate as excipient				32.1 ± 1.4

were magnetically stirred at 750 rpm for 24 h at room temperature. The obtained suspensions were filtered through a 0.22 µm nominal pore size PES membrane syringe filter. The amounts of KBAs, AKBAs, βBA and AβBA in the filtrates were measured by HPLC.

Preparation of solid dispersions and physical mixtures

Solid dispersions (SDs) of BSE with 20% (w/w) nominal ΣBA content (sum of KBAs, AKBAs, αBA, βBA, AαBA and AβBA) were prepared *via* lyophilization with γ-CD, HP-β-CD and HP-γ-CD at a weight ratio of 1:1 (accurate weights and assays are summarized in Table 3). First, 150 mg/mL CD solutions were prepared (on a dry basis) with 20 mL PW in round bottom flasks. Second, an appropriate amount of BSE was added and magnetically stirred (750 rpm) for 24 h. The suspensions were frozen in an acetone bath cooled with dry ice (−77 °C) under continuous stirring to obtain an even layer of the frozen cake. The samples were lyophilized for 24 h at room temperature (25 ± 2 °C) using a ScanVac Coolsafe 55-4 (LaboGene A/S, Lillerød, Denmark) apparatus equipped with a BOC Edwards E2M28 (BOC Edwards, Burgess Hill, UK) vacuum pump (0.1 mbar maintained throughout 24 h). Finally, the cakes were broken and sieved at 630 µm and 500 µm pore sizes. Physical mixtures (PMs) were also prepared in a mortar and sieved at the same pore sizes followed by additional homogenization.

Solid-state analysis

Powder X-ray diffraction (P-XRD)

Powder XRD measurements were performed using a PANalytical X'Pert PRO diffractometer (Malvern Panalytical, Worcestershire, UK) equipped with a Cu Kα radiation source (λ_1 = 1.5406 Å, λ_2 = 1.5444 Å) operating at 40 kV and 30 mA. Data were collected in a continuous scan mode over a 2θ range of 4.0° to 84.0° with a step size of 0.0167° and a time of 5.08 s per step. A Bracket Flat Stage sample holder was used, and measurements were conducted in a θ–θ geometry (PW3050/60 goniometer) without the use of a monochromator.

Differential scanning calorimetry (DSC)

DSC measurements were performed on a Discovery DSC 2500 (TA Instruments, New Castle, DE, US) under flowing nitrogen (50 mL/min cell purge; 300 mL/min base purge) with a heating rate of 10 °C/min between 40 °C and 320 °C. Solid samples of 3.0–8.0 mg were weighed into Tzero aluminum pans. The melting point of the samples was determined before the DSC analysis using a BÜCHI Melting Point B-450 (Büchi Labortechnik, Flawil, Switzerland) apparatus. The results were normalized by accurate weighing.

Attenuated total reflectance fourier-transform infrared spectroscopy (ATR FT-IR)

FTIR spectra of the SDs were analyzed using a Jasco 4600 FT-IR spectrometer equipped with an ATR (Pro One) accessory. An appropriate amount of each powdered sample was placed on the ATR crystal

(ZnSe) and the spectra were acquired over the range of 4000–500 cm^{-1} at a resolution of 4 cm^{-1} with 32 scans per sample to improve the signal-to-noise ratio. Background spectra were automatically subtracted by Spectra Manager (v2.15.01).

In vitro *mini dissolution*

The *in vitro* release profiles of the formulations were investigated in fed- and fasted-state simulated intestinal fluid media, prepared according to the manufacturer's guidelines. For each experiment, the samples were accurately weighed to obtain a final dispersion in 8 mL of the respective dissolution medium containing 8 mg of total boswellic acid content (ΣBA; sum of major BAs, including KBAs, AKBAs, αBA, βBA, AαBA and AβBA), corresponding to a concentration of 1 mg/mL BA in the digest. Dissolution was performed at 37 °C under constant shaking at 1000 rpm with a Heidolph Titramax 1000 (Heidolph Instruments, Schwabach, Germany). Aliquots of 100 µL were withdrawn at 5, 15, 30, 60, 120, and 240 min. Each aliquot was immediately centrifuged at 4500 rpm for 5 min, and 5 µL of the clear supernatant was analyzed by HPLC. The percentage of BAs released over time was calculated, and the results were expressed as mean ± standard deviation (SD). Each dissolution was conducted in triplicate.

The dissolution of BAs at a given timepoint (*t, min*) in % was calculated using **Equation 1**.

$$\textbf{Dissolution of BAs}\,(\%) = \left(\frac{\textbf{Total BA in solubilised form}}{\textbf{Total BA dose}}\right)\times\textbf{100}) \tag{1}$$

The *in vitro* food effect of the samples was calculated using **Equation 2** (Mathias et al. 2015).

$$\textit{Food Effect}\,(-) = \frac{AUC_{Fed}}{AUC_{Fasted}} \tag{2}$$

Where the AUC_{Fed} and AUC_{Fasted} are the area under the curve of the fed- and fasted-state dissolution (0–240 min), respectively (calculated using the trapezoidal method).

Intestinal parallel artificial membrane permeability assay (intestinal-PAMPA)

PAMPA studies were conducted using the Gut-Box™ apparatus (Pion Inc., Riverside, UK) thermostated at 37 °C. The applied doses were identical to those in the dissolution studies (1 mg/mL ΣBA in digest). Each well of the MultiScreen-IP filter plates acceptor plate was coated with 5 µL lipid solution: 16 mg phosphatidylcholine, 4 mg cholesterol dissolved in a 600 µL solvent mixture of dodecane/hexane/chloroform 25/70/5% (V/V). The donor compartment (below) was filled with the samples (L1, L2 and REF) suspended in 300 µL FaSSIF pH 6.5 and FeSSIF pH 5.8 with stirring disks (set to 60 µm unstirred water layer). The acceptor compartment (above) was filled with 250 µL 25 mg/mL HP-γ-CD solution prepared in PBS pH 7.4 to provide double-sink conditions (pH and complexation) (Avdeef 2003).

Permeation was assessed over 120 min, with sampling at 15, 30, 60 and 120 min. BAs concentrations in the acceptor and donor phases were measured by HPLC after appropriate dilution. Donor samples were filtered through a MultiScreenHTS-PCF filter plate (0.45 µm pore size) prior to dilution. The apparent permeability (P_{app}, in 10^{-6} cm/s) of each compound was calculated using **Equation 3**, applying the precipitated-donor model (infinite donor reservoir) (Avdeef 2003).

$$P_{app} = -\frac{2{,}303\cdot V_A}{A\left(t-\tau_{lag}\right)}\cdot\log\left(1-\frac{C_A(t)}{S(t)}\right) \tag{3}$$

where V_A is the volume of the acceptor phase (0.250 mL), A is the accessible surface of the membrane (corrected with porosity, 0.24 cm^2), t is the duration of permeation in seconds, τ_{lag} is the time required to saturate the membrane with solute (with this membrane type it is considered negligible compared to the sampling points), $C_A(t)$ is the concentration of BAs in the acceptor phase at a given timepoint, and $S(t)$ is the concentration of BAs in the donor phase (equivalent to its solubility) at a given timepoint. The optimal timepoint to calculate P_{app} was determined based on the concentration-time curves of the donor and acceptor phases. The optimal timepoint is in the early kinetic stage where only a small fraction of the molecules has permeated. The percentage of permeated BAs at each timepoint was calculated using **Equation 4**.

$$\textbf{Permeated fraction of BAs}\,(\%) = \left(\frac{\textbf{mass of BAs in acceptor}}{\textbf{Dose of BAs}}\right) * 100 \tag{4}$$

Ex vivo *permeation on porcine small intestine*

Ex vivo permeation studies were conducted on porcine small intestine. The intestine was cleaned and sectioned into 10 cm segments, immersed in physiological saline, and promptly frozen.

These segments were vertically opened, divided into three equal parts, and shaped into round pieces to suit the permeation apparatus. The membrane was inserted into the permeation device with the apical side oriented toward the donor compartment and sealed with a Teflon ring to provide an identical permeation area (0.196 cm^2).

9 mL cells were used for both the donor and acceptor compartments in a side-by-side type horizontal permeation system. Formulations were vortexed for 15 s in FaSSIF pH 6.5 solution and thereafter transferred to the donor cell. The acceptor was filled with 25 mg/mL HP-γ-CD solution prepared in PBS pH 7.4 buffer. Permeation was performed for 240 min at 37 °C. Aliquots of 100 µL were withdrawn from the acceptor at given timepoints and were immediately replaced with the acceptor medium. The experiments were performed in triplicate. Following permeation, the tissues were extracted using 10 × 1 mL ACN. The solutions were then evaporated using a Stuart Sample Concentrator SBHCONC/1 (Stone, Staffordshire, UK) with continuous flow of N_2 at 25 °C. The obtained samples were reconstituted in ACN, filtered and analyzed for the concentrations of KBAs and AKBAs using HPLC. Finally, the tissues were dried (40 °C, 0.1 bar) until a consistent mass was obtained for the estimation of their dry weight.

Cumulative amount $Q(t)$ (µg) of KBAs and AKBAs in the acceptor compartment was calculated using **Equation 5**.

$$\boldsymbol{Q}_i\,(\mu g) = \boldsymbol{C}_i \cdot \boldsymbol{V}_A + \boldsymbol{\Sigma}_{j=1}^{i-1} \boldsymbol{C}_j \cdot \boldsymbol{V}_s \tag{5}$$

Wherein C_i is the acceptor concentration at time i (µg/mL), V_A is the volume of acceptor well (9 mL), C_j is the concentration of BAs in the earlier samples taken, Vs is the sampling volume (0.1 mL). The amounts of KBAs and AKBAs were summed as $Q(t)_{total}$.

The steady-state flux (J_{ss}) was calculated using **Equation 6.**

$$\boldsymbol{J}_{ss}\left(\frac{\mu g}{cm^2}/min\right) = \frac{\left(\frac{dQ}{dt}\right)}{A} \tag{6}$$

where dQ/dt is the slope of the linear region of the cumulative curve for the BAs separately, and A is the permeation area (0.196 cm^2).

The apparent membrane retention MR_{app} (%) was calculated using **Equation 7.**

$$\mathbf{MR}_{\mathbf{app}}\,(\%) = \frac{\boldsymbol{m}_{\mathbf{membrane}}}{\boldsymbol{m}_{\mathbf{don,eq}} + \boldsymbol{m}_{\mathbf{acc}} + \boldsymbol{m}_{\mathbf{membrane}}} * 100 \tag{7}$$

where $m_{membrane}$ is the mass of BAs extracted from the membrane, $m_{don,eq}$ is the mass of solubilized BAs in the donor phase at equilibrium and m_{acc} is the mass of BAs in the acceptor phase after 240 min.

Stability studies

Accelerated stability studies were initiated in sealed glass headspace vials in accordance with ICH Q1A(R2) guidelines to assess the physical and chemical stability of the preformulations.

The samples were stored in two conditions (Memmert Constant climate chamber HPP110ECO, Büchenbach, Germany): at 25 ± 2 °C with 60 ± 5% relative humidity (RH) and at 40 ± 2 °C with 75 ± 5% RH, protected from light. Samples underwent visual and physical examination, as well as HPLC analysis after 0, 1, 3 and 6 months. The shelf-life of the intermediate products ($t_{90\%}$) was estimated using a zero-order kinetic model.

Statistical analysis

Statistical analyses were performed using Python (*Statsmodels*, and *Scikit-posthocs*). Dissolution data were analyzed separately for each dissolution medium using one-way analysis of variance (ANOVA), followed by Dunnett's post hoc test to compare each formulation with BSE and the REF. All other data were analyzed using Welch's t-test, with Holm correction to account for multiple comparisons. Data are presented as mean ± SD.

Results and discussion

Structure elucidation of isolated compounds

Chromatographic separations of the acidic fraction obtained from the steam distillation by-product of *B. sacra* yielded major BAs, listed in Supplementary Materials, Table S1. The identification of the compound was achieved by comparison of its ^{1}H NMR spectroscopic data with those reported in the literature. The structures of BAs are presented in Figure 1. ^{1}H-NMR spectra of the isolated compounds are available in the (Supplementary Materials Figures S3–S8).

HPLC analysis

The chemical characterization of BSE and corresponding formulations has been performed using HPLC analysis. The retention times (Rt) were as follows: KBAs – 4.29 min, AKBAs – 6.85 min, αBA – 9.54 min, βBA – 10.13 min, AαBA– 14.50 min, and AβBA – 14.74 min as shown in Figure 2.

Previous study reported that alpha and beta constitutional isomers of KBA and AKBA may not be separated under reversed-phase conditions (Schmiech et al. 2021). As a result, the analytes of α and β isomers are collectively referred to as KBAs and AKBAs in the extract. The chemical composition of BSE has been determined by the quantification of major BAs, as shown in Table 4.

Cyclodextrin screening

The solubility of BAs present in BSE was markedly limited in PBS at pH 7.4 (Table S2), quantified at 0.002, 0.010, 0.005, and 0.004 mg/mL for KBAs, AKBAs, βBA, and AβBA, respectively. As shown in Figure 3, native α- and β-CD exerted little or no effect on BA solubility, while SBECD produced only moderate improvements across the individual BAs. HP-β-CD, one of the most widely used CDs, also enhanced solubility only to a moderate extent, although consistently

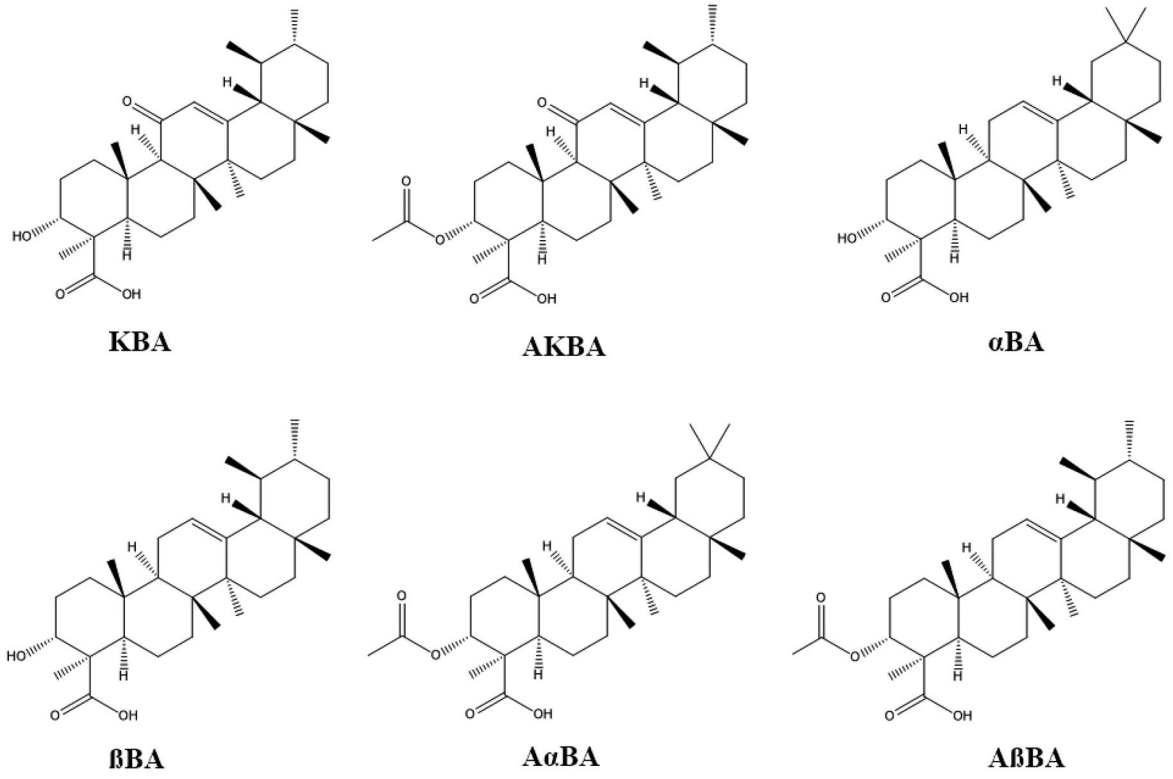


Figure 1. Structure of the isolated compounds: KBA: 11-keto-β-boswellic acid; AKBA: 3α-*O*-acetyl-11-keto-β-boswellic acid; αBA: α-boswellic acid; βBA: β-boswellic acid; AαBA: 3-*O*-acetyl-α-boswellic acid; AβBA: 3-*O*-acetyl-β-boswellic acid.

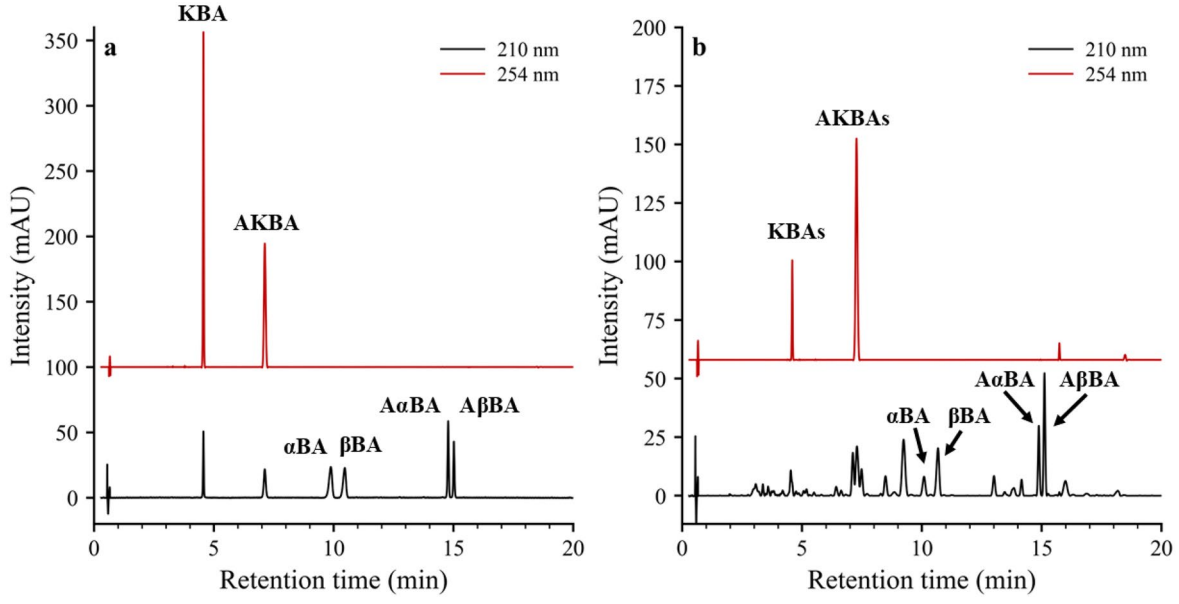


Figure 2. HPLC chromatogram of the standards (a) and *B. serrata* extract (b). KBAs and AKBAs detected at 254 nm (red), other BAs at 210 nm (black).

for all examined boswellic components. In contrast, the methylated and hydroxypropylated γ-CD derivatives produced a pronounced increase in apparent solubility of BAs, with RAMEG providing the greatest enhancement and HP-γ-CD also substantially outperforming the corresponding β-CD derivatives. An interesting exception was the native γ-CD, which reduced the apparent solubility of BAs. This behavior was confirmed visually, by the formation of a fine white suspension and

Table 4. Boswellic acid composition of BSE in % (w/w) expressed as mean ± SD ($n = 6$).

Boswellic Acid	Content % (w/w)
KBAs	1.4 ± 0.1
AKBAs	7.9 ± 0.2
αBA	3.2 ± 0.2
βBA	8.1 ± 0.3
AαBA	5.1± 0.2
AβBA	12.9 ± 0.7
ΣBA	38.6 ± 0.5

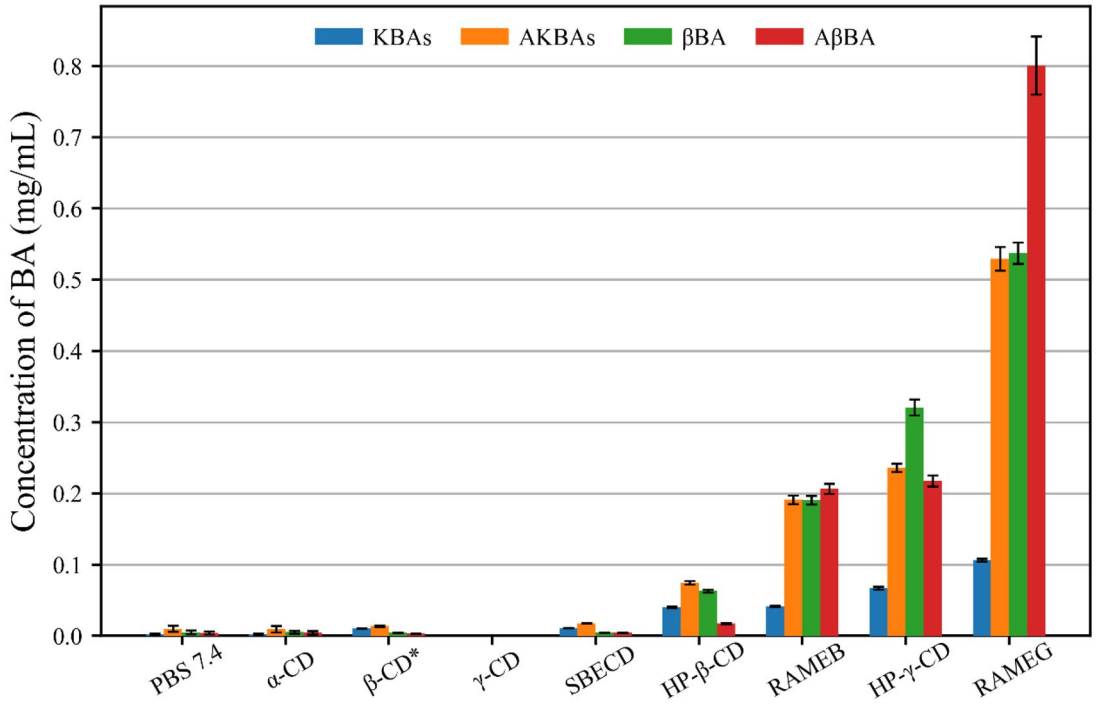


Figure 3. Solubility of BAs present in BSE in pbs pH 7.4 buffer and 50 mM CD solutions (*in case of β-CD, only 12 mM) ($n = 3$).

analytically, by the absence of detectable BAs in the filtrate, indicating the formation of poorly soluble inclusion complexes.

The greater apparent solubilization observed with γ-CD derivatives is consistent with the hypothesis that the larger γ-CD cavity may better accommodate the bulky, pentacyclic BA structures. However, since host–guest interactions were not directly characterized, the contribution of cavity size remains tentative. Within both CD families, randomly methylated derivatives exhibited greater solubilizing capacity than the corresponding hydroxypropyl derivatives, suggesting that substituent type also influences solubilization. The superior performance of methylated CDs is likely related to their enhanced hydrophobicity and reduced intermolecular hydrogen bonding, which increase the accessibility of the CD cavity and promote stronger interactions with the highly lipophilic BAs. Despite its superior solubilizing effect, RAMEG was excluded from further development due to the lack of regulatory approval for pharmaceutical use. Similarly, RAMEB, although more effective than HP-β-CD, was not pursued further for oral applications due to regulatory constraints. Nevertheless, native γ-CD was retained for further investigation because the initially formed insoluble complexes may exhibit improved dissolution behavior upon dilution (Schönbeck et al. 2017). Consequently, subsequent studies focused on pharmaceutically acceptable CD systems, primarily the native γ-CD, HP-γ-CD and HP-β-CD.

Preparation of solid dispersions and physical mixtures

Based on the CD screening results, the best-performing CDs were selected to prepare BSE formulations for oral delivery. Solid dispersions of BSE containing 20% (w/w) nominal ΣBA content were prepared by lyophilization (L) and physical mixing (F) of γ-CD (L1, F1), HP-γ-CD (L2, F2) and HP-β-CD (L3, F3) with BSE in a 1:1 weight ratio. HPLC analysis indicated that the ΣBA content of the samples was consistent with the nominal value within experimental error. The results of the HPLC assay are summarized in Table 3.

Solid-state analysis

The prepared SDs were analyzed using FT-IR, PXRD and DSC. The complete datasets are provided in the (Supplementary Materials Figure S9).

For the HP-γ-CD (L2, F2) and HP-β-CD (L3, F3) systems, the applied solid-state analytical techniques revealed predominantly amorphous materials and only minor differences between the PMs and the corresponding lyophilized samples. PXRD patterns showed broad amorphous halos without characteristic crystalline reflections, while DSC thermograms largely reflected the thermal behavior of the starting materials. Likewise, FT-IR spectra showed only limited spectral changes in the lyophilized samples. Overall, these findings derived from the applied solid state analysis techniques indicate that lyophilization did not induce substantial solid-state modifications in the BSE-hydroxypropyl-CD systems. In contrast, the native γ-CD-based lyophilizate (L1) exhibited pronounced solid-state changes and is therefore discussed in detail below (Figure 4a–c).

The FT-IR spectra of the γ-CD-based samples are shown in Figure 4a. The FTIR spectrum of the PM (F1) largely retained the characteristic spectral features of the individual starting materials, indicating that simple blending did not substantially alter their molecular environments. In contrast, the lyophilized system (L1) showed spectral alterations including shifts and intensity reductions of the characteristic stretching vibrations of C-H (2850, 2922 cm^{-1}) and carbonyl (1702 cm^{-1}) bands of BSE. These observations suggest modifications in the local molecular environment of the lyophilized BSE-γ-CD system. However, FT-IR spectroscopy alone does not allow definitive conclusions regarding the nature of the intermolecular interactions involved (Szente 1996).

The PXRD results are presented in Figure 4b. BSE was predominantly amorphous, with two distinct peaks at 27° and 41°, attributed to residual KCl originating from the extraction process. Native γ-CD exhibited a characteristic crystalline diffraction pattern. In the PM, the γ-CD reflections remained visible, although with reduced intensity due to dilution by BSE. In contrast, the diffractogram of L1 revealed complete disappearance of the γ-CD crystalline reflections and the appearance of a broad diffuse halo, indicating loss of crystallinity and formation of an amorphous solid-state system.

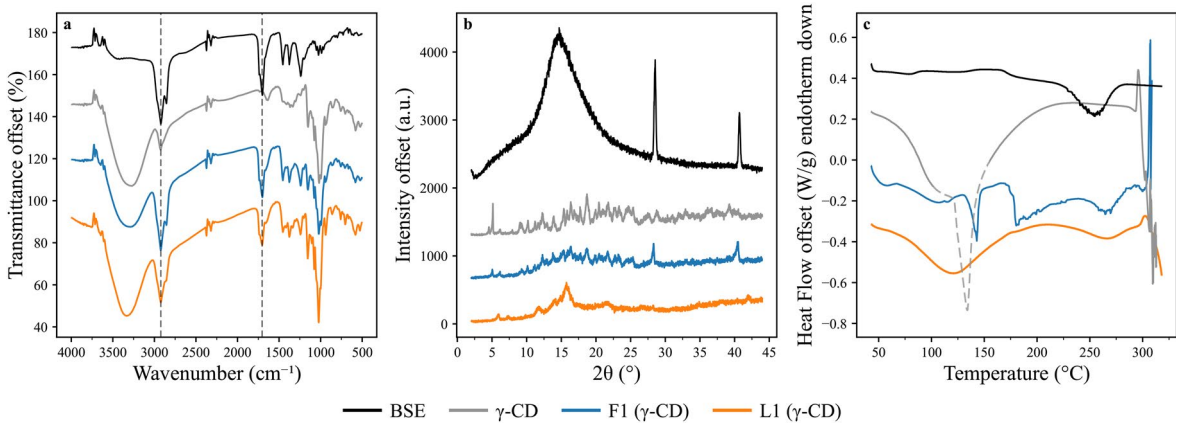


Figure 4. (a) FT-IR Spectra and (b) P-XRD patterns of BSE, native γ-CD, F1 and L1. (c) DSC thermograms of BSE, native γ-CD, F1 and L1. Complete FT-IR, PXRD and DSC datasets are provided in the (supplementary Materials Figure S9).

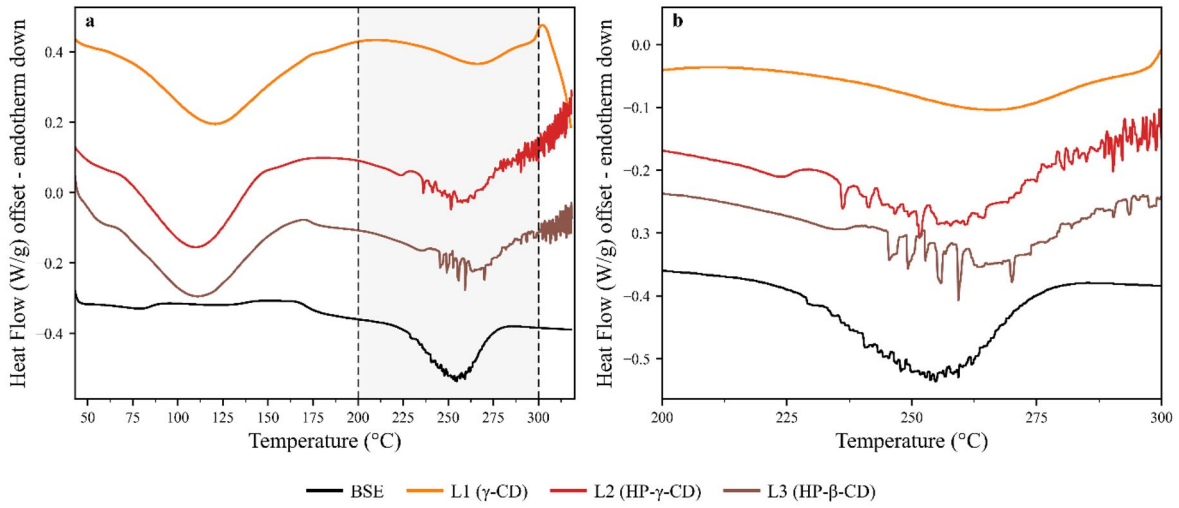


Figure 5. (a) DSC thermograms of BSE and the lyophilized systems, (b) thermogram enlarged in the range of 200-300 °C.

The DSC results in Figure 4c illustrate that the native extract had a minor thermal transition around 171 °C, followed by a broad endothermic event associated with decomposition starting at approximately 230 °C. Native γ-CD showed a wide endothermic event associated with dehydration between 70 and 150 °C, with a distinct minimum at 135 °C, followed by degradation-related thermal events occurring over 290 °C. The PM F1 largely combined the thermal features of BSE and γ-CD, including the γ-CD dehydration event and high-temperature degradation behaviors. In contrast, the lyophilized sample (L1) showed a delayed and less intense thermal response relative to both the initial materials and F1. Most notably, the endothermic decomposition peak characteristic of BSE disappeared, suggesting that BSE was no longer a thermally isolated phase but was incorporated into a novel amorphous BSE–γ-CD matrix.

Additionally, the thermograms of all lyophilized samples (L1, L2, L3) are compared in Figure 5a, with an enlarged view of the 200-300 °C range shown in Figure 5b. In contrast to L1, the L2 and L3 systems showed thermograms that closely resembled those of BSE with no comparable changes observed.

While FT-IR and P-XRD provided supportive information, neither technique alone was sufficiently diagnostic to confirm complex formation in this multicomponent system. DSC offered the clearest evidence of intermolecular interactions, as the thermal behavior of the lyophilized BSE–γ-CD system differed markedly from that of both the PM and the individual components. When interpreted collectively, the data indicate the formation of a novel amorphous solid-state system with a modified molecular environment, consistent with inclusion complex formation (Mura 2015).

In vitro *mini-dissolution in biorelevant media*

The dissolution profiles of the formulations are summarized in Figure 6.

In FaSSIF medium, native BSE exhibited limited dissolution, achieving only 2.5% ± 0.4% BAs release after 240 min, confirming the poor solubility of BAs under fasted intestinal conditions (Sharma and Jana 2020). The REF demonstrated moderate release of 5.8% ± 0.2%, significantly (Dunnett's post hoc, $p < 0.01$) surpassing the native extract. All CD-based formulations showed significant enhancements in dissolution relative to REF (Dunnett's post hoc, $p < 0.001$), apart from the PM (F3). Among the lyophilized formulations, L1 and L2 had the highest release extents, reaching 19.2% ± 0.2% and 20.5% ± 0.4%, respectively, which corresponds to an approximate eight-fold increase compared to the native BSE. Specifically, L1 showed rapid initial release kinetics, reaching 17% ± 0.3% after 15 min, whereas L3 reached only ~12.4% release at 240 min. Notably, both γ-CD-based PMs (F1, F2) reached a higher degree of dissolution compared to HP-β-CD lyophilisate (L3), hence supporting the hypothesis that a larger CD cavity may favor BA dissolution.

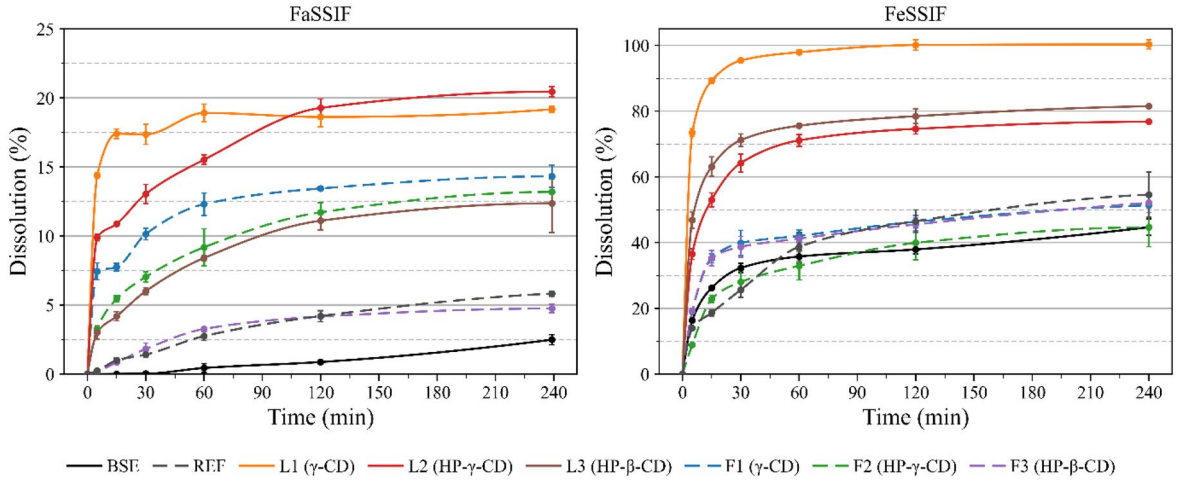


Figure 6. *In Vitro* dissolution profiles of BSE, the REF and formulations in FaSSIF and FeSSIF media ($n = 3$).

The dissolution profiles in FeSSIF medium were notably superior across all tested formulations compared to FaSSIF, reflecting the enhanced solubilization capacity of FeSSIF due to its significantly higher bile salt and lecithin content (approximately 5–10 times of FaSSIF). Native BSE achieved moderate dissolution, releasing 44.7% ± 2.5% of BAs at 240 min. The lyophilized samples displayed significantly improved dissolution (Dunnet's post hoc, $p < 0.001$), particularly the L1 complex, which achieved rapid and near-complete release of 102.3% ± 1.3% at 240 min, with 95% dissolved within the first 30 min. The L2 and L3 formulations demonstrated significantly (Dunnet's post hoc, $p < 0.001$) enhanced release, reaching 76.7% ± 0.4% and 81.5% ± 0.4% respectively. In contrast, the PMs demonstrated moderate to negligible improvements (Dunnet's post hoc, $p > 0.118$) compared to BSE. The REF reached a notable dissolution of 54.6% ± 6.9% by 240 min, surpassing that of the native BSE and PMs, but it remained lower than those of all lyophilized CD samples.

Interestingly, a medium-dependent shift was observed in FeSSIF, with L3 surpassing L2, suggesting an interaction between HP-γ-CD and bile salt components that limits its solubilizing capacity. Visual observations supported this, as L2 formed aggregates in FeSSIF, a behavior not seen in FaSSIF or with other formulations. These interactions may reduce the solubilizing ability of hydroxypropylated CDs by occupying the CD cavity and displacing the guest molecule, while also reducing the accessible surface area after aggregation (Cuoco et al. 2023). Our findings align with literature emphasizing the poor solubilization ability of FaSSIF for highly lipophilic compounds and the recommendation to administer BSE after a meal (Sterk et al. 2004). The food effect (AUC_{Fed}/AUC_{Fasted}) was reduced from 35 of the native BSE to only 5 and 4 with L1 and L2, respectively. Overall, the results demonstrate advantages of selected γ-CD formulations over HP-β-CD under tested dissolution conditions. Among the investigated CDs, the native γ-CD provided the most favorable dissolution profiles in both media, despite reducing the apparent solubility in the CD screening experiment. This apparent discrepancy supports the hypothesis that the poorly soluble inclusion complexes formed at high CD concentrations readily dissociate upon dilution, thereby enhancing drug release under biorelevant conditions (Schönbeck et al. 2017).

In vitro *permeability study – intestinal-PAMPA*

In accordance with the dissolution studies, two lyophilized samples (L1, L2) and the REF were selected for PAMPA testing to evaluate the apparent permeability of BAs in FaSSIF and FeSSIF media.

In FaSSIF, the cumulative permeation profiles (Figure 7a) showed a constant linear increase, suggesting robust membrane integrity and maintained sink conditions during the experiment. Both CD-based formulations exhibited higher transport than REF throughout the experiment, with the highest differences observed at early timepoints (up to 5-fold increase at 30 min). Although L2 provided the highest permeation, the difference between L1 and L2 was minor and decreased over time.

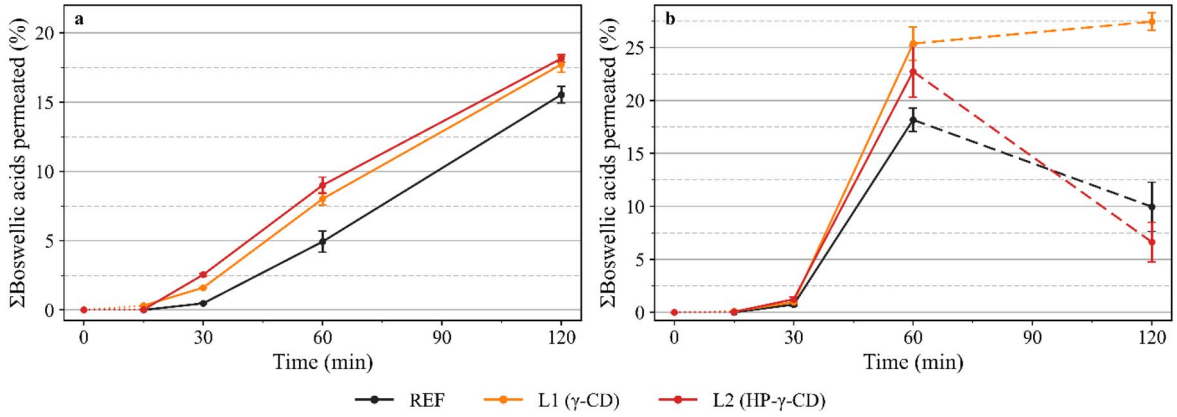


Figure 7. Total permeated fraction of BAs (% of ΣBA dose) over time in FaSSIF (a) and FeSSIF (b) media ($n = 3$).

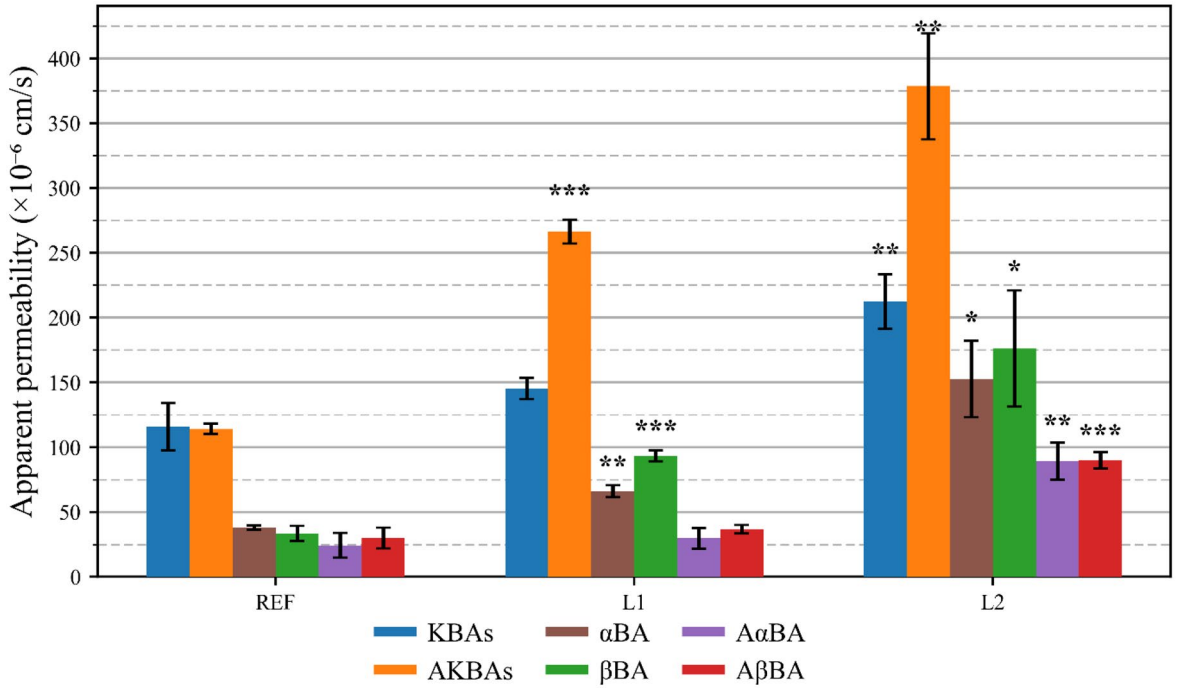


Figure 8. Apparent permeability of BAs in FaSSIF media at 30 min. Asterisks indicate significant differences compared to the REF (welch's t-test, *$p = <0.05$; ** $p < 0.01$; *** $p < 0.001$, $n = 3$).

In FeSSIF, the permeation profiles (Figure 7b) showed limited permeation for up to 30 min in contrast to FaSSIF. This was followed by a rapid increase, a plateau and subsequent decline, accompanied by increased variability. This behavior suggests an imbalance in membrane integrity, insufficient sink conditions and reverse flux. Thus, the present PAMPA setup may not sufficiently simulate fed-state conditions as the high bile salt and lecithin content of the FeSSIF donor media may damage the artificial membrane. Accordingly, the FeSSIF PAMPA data are considered descriptive only and are not used to infer physiological fed-state absorption or rank formulations; quantitative P_{app} comparisons are restricted to FaSSIF.

The apparent permeability values of the individual BAs were calculated at the 30-min time point in FaSSIF media (Figure 8 and Table S3). For most compounds, both CD-based formulations showed significantly (Welch's t-test, $p < 0.05$) higher P_{app} values than REF, with L2 surpassing L1 as well. The apparent permeability was over 2- and 3-fold higher for KBAs and AKBAs in the L2 sample compared to the REF. The improvement was less pronounced for the L1 with about 1.5- and 2.5-fold for the two major bioactive compounds, respectively.

The reported P_{app} values should be interpreted as formulation-dependent apparent permeability coefficients rather than intestinal effective permeability (P_{eff}) or direct measures of intrinsic membrane permeability. Although Equation 3 accounts for the measured donor concentration, this concentration does not distinguish between unbound, CD-associated, micelle-associated and other solubilized BAs. CD-mediated solubilization may increase the amount of BAs maintained in the dissolved donor pool and facilitate their transport across the unstirred water layer by increasing the availability of dissolved drug near the membrane surface (Loftsson and Brewster 2011). However, complex formation may also affect the unbound fraction available for membrane partitioning. In addition, the presence of bile salts further complicates the interpretation of the PAMPA results, as bile salts not only form micelles with the BAs but can show competitive behavior for the CD cavity resulting in the displacement of the drug (Eriksen et al. 2022; Cuoco et al. 2023). Since these contributions cannot be separated based on the present data, the higher P_{app} values indicate enhanced apparent transport under the tested conditions but do not establish increased intrinsic membrane permeability. Quantification of unbound donor concentrations alongside transport measurements would be required to distinguish changes in solubilization from changes in intrinsic permeability in this multicomponent system.

Interestingly, the substantial apparent permeability observed in our FaSSIF PAMPA model contradicts the results of an earlier PAMPA model where permeability of the individual BAs was very limited (Sharma and Jana 2020). However, the two PAMPA models are incomparable for multiple reasons: the infinite (precipitated) donor reservoir model assumes that the donor is saturated with the analyte during the experiment; the composition of the artificial membrane varies and the use of different complexing agents as sink can result in significant differences in apparent permeability. BAs are classified as BCS IV compounds, characterized by their low solubility and permeability. They are extremely lipophilic molecules, with *logP* values between 5 and 7. Inadequate sink conditions strongly increase the risk of membrane retention and saturation of the acceptor compartment, which may contribute to an underestimation of permeability (Angi et al. 2025). Moreover, the incorporation of a complexation agent (i.e., CDs) in the acceptor phase mimics blood circulation and plasma protein binding; this is particularly important for BAs, especially AKBAs and KBAs, which exhibit high plasma protein binding (Abdel-Tawab et al. 2011). Overall, these findings highlight the importance of donor-phase solubilization and assay conditions in determining apparent BA permeability. In complex CD- and bile-salt-containing media, dissolution and transport should be evaluated together (Eriksen et al. 2022). The relative contributions of solubilization and intrinsic membrane permeability remain unresolved, and these results cannot directly establish intestinal absorption *in vivo*.

Ex vivo *permeation on porcine small intestine*

In accordance with the established *ex vivo and in vivo* literature on BA derivatives, as revealed through an exhaustive review (Table 1), and considering the *in vitro* penetration results from our current study along with the related quantitative analytical limitations, our *ex vivo* investigations were exclusively focused on the KBAs and AKBAs, which are the most commonly evaluated pharmacokinetic markers. The cumulative *ex vivo* permeation profiles of KBAs and AKBAs in L1, L2 and REF are summarized in Figure 9. These demonstrate a notable enhancement for both CD-based formulations, with L1 showing the highest increase (~15-fold), followed by L2 (~3-fold) in comparison to the REF. L1 exhibited a sustained, nearly linear increase across the duration, suggesting prolonged steady-state flux devoid of evident transport limitations. In contrast, L2 deviated from linearity earlier and gradually approached a plateau, indicating the onset of transport limitations. Importantly, the total permeated fraction remained low relative to the applied dose (below 8% for KBAs in L1), indicating preserved tissue integrity throughout the experiments.

The observed trends are reflected in the steady-state flux values (Figure 10a,b) derived from the initial linear phase (0–60 min), during which both the L1 and L2 significantly (Welch's t-test, $p < 0.05$) increased the flux of KBAs and AKBAs compared to the reference, with L1 surpassing L2 as well. The calculated apparent membrane retention data (Figure 10c,d) further support this

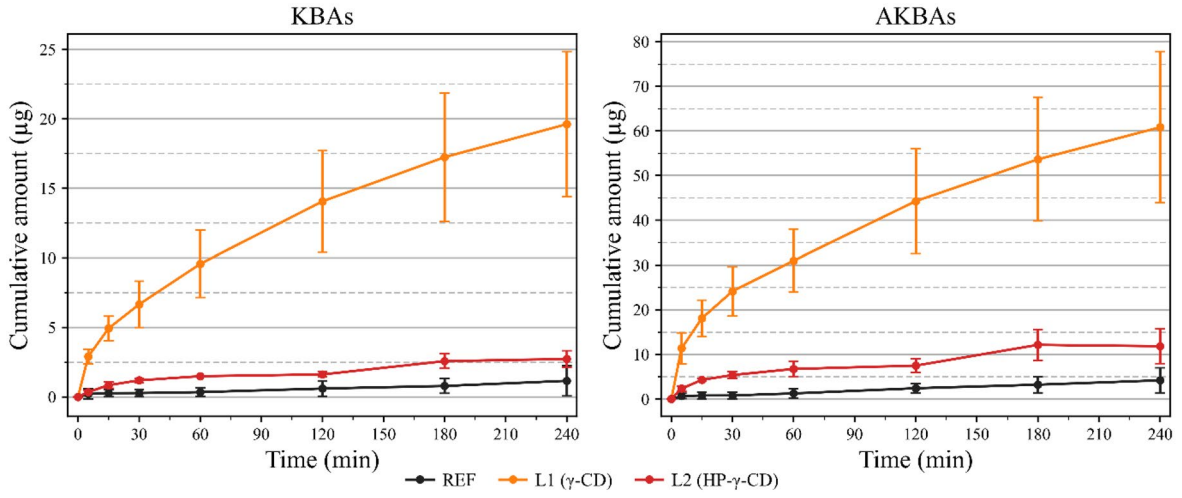


Figure 9. *Ex vivo* permeation. Cumulative amount of KBAs (left) and AKBAs (right) in the acceptor phase over time ($n = 3$).

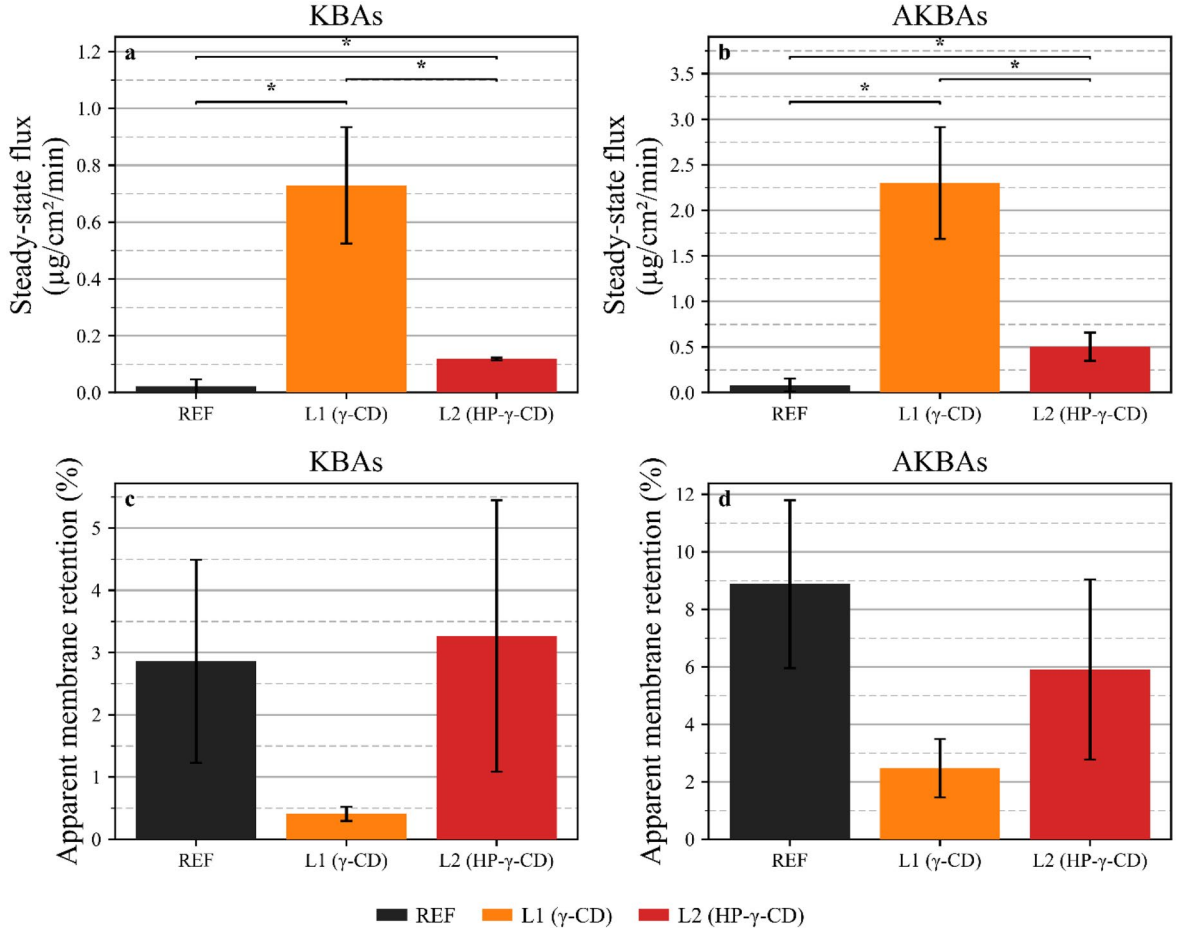


Figure 10. Steady-state flux of KBAs (a) and AKBAs (b). Apparent membrane retention of KBAs (c) and AKBAs (d). Asterisks (*) indicate significant differences compared to the REF (Welch's t-test, $p < 0.05$, $n = 3$).

interpretation, since L2 led to substantially higher accumulation of BAs inside the tissue, indicating higher retention and membrane affinity, which limited effective translocation. In contrast, L1 achieved higher permeation with less membrane accumulation, indicating enhanced transmembrane transport efficiency.

These findings notably contrast with the PAMPA results, where L2 showed higher apparent permeability, highlighting fundamental differences between the two models. While both models reflect passive partition-driven processes, PAMPA uses a thin, simplified artificial membrane consisting of cholesterol and phosphatidylcholine dissolved in dodecane. Whereas the *ex vivo* system uses a thick, multicellular tissue comprising several cell layers rather than a single lipid barrier. The epithelial barrier is composed of tissue-specific lipids and membrane proteins, providing a much more physiologically relevant permeability barrier. In addition, the presence of an overlying mucus layer rich in mucins further influences drug diffusion and permeation, a feature that is absent in the PAMPA model. In this context, L1 appears to support a more efficient transcellular permeation, potentially reflecting a favorable balance between solubilization and release at the membrane site. Although L2 exhibited superior dissolution in FaSSIF, the effective free drug fraction may have been lower, thereby limiting net permeation. These findings demonstrate that improved dissolution alone does not necessarily translate into enhanced permeability; rather, efficient transmembrane transport depends on the interplay between solubilization, free drug availability, and membrane interactions. The reversed ranking of L1 and L2 remains mechanistically unresolved; the proposed explanations require further targeted investigation.

Stability studies

The stability of CD-based formulations (L1, L2) was markedly improved compared to the native extract. The unformulated extract showed physical and chemical instability (especially in the first month), characterized by a visible color change and solidification into a glassy, resinous mass under both conditions. In contrast, as seen in Figure 11, both L1 and L2 remained physically stable, preserving their powder characteristics. The predicted shelf-life ($t_{90\%}$) under normal conditions (25 °C, 60% RH) increased from 4.9 months for BSE to 11.8 months for L1 and 8.6 months for L2 (Figure S10, Table S4). A greater increase was observed under accelerated conditions (40 °C, 75% RH), with the $t_{90\%}$ of BAs rising from 2.4 months for the native extract to 7.6 and 6.9 months for L1 and L2, respectively. The results show that the unformulated extract is prone to rapid degradation and CD complexation markedly enhances the stability of BAs, with the native γ-CD providing the most robust protection by maintaining both physical integrity and chemical composition over prolonged durations.

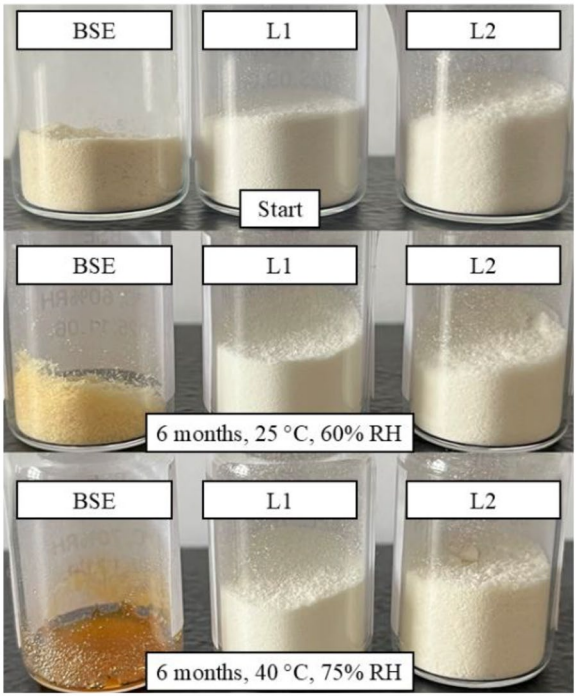


Figure 11. Visual inspection of BSE, L1 and L2 after 6 months at normal and accelerated conditions.

Although enhanced systemic exposure often improves the *in vivo* anti-inflammatory efficacy of BSE formulations, higher plasma concentrations do not necessarily translate into superior pharmacological effects (Schmiech et al. 2024). This discrepancy suggests that formulation-dependent factors may influence therapeutic outcomes independently of systemic exposure. Furthermore, many advanced delivery systems are associated with increased formulation complexity, stability challenges, limited long-term safety data, and uncertain translational potential despite their promising pharmacokinetic performance (Rutkowska and Olszewska 2026). Conversely, CDs are well-established pharmaceutical excipients with favorable safety profiles and regulatory acceptance. While advanced nanocarriers may be advantageous for applications requiring tissue targeting or controlled drug release, CD complexation represents a pragmatic formulation strategy when the primary objective is to improve the apparent solubility and oral absorption of BSE while maintaining low formulation complexity.

The present findings extend, rather than contradict, the β-CD-focused studies of Tambe et al. (2018, 2019). These earlier studies demonstrated the advantages of β-CD- and HP-β-CD-based formulations for improving the solubilization, dissolution and apparent intestinal permeation of BAs, identifying HP-β-CD as a promising carrier among the systems investigated. However, γ-CD carriers were not included in those comparisons. Differences in formulation composition, extract matrix and experimental conditions should also be considered: Tambe et al. (2019) examined AKBA transport from a total BA fraction using rat everted gut sacs, whereas the present study used an in-house BSE acidic fraction, biorelevant dissolution, PAMPA and porcine intestinal tissue. Furthermore, differences in extract composition and matrix complexity may influence cyclodextrin interactions, dissolution behavior and the availability of individual BAs for permeation, potentially contributing to the differences observed between studies. The present study broadens the comparison by evaluating native γ-CD and HP-γ-CD alongside HP-β-CD in the dissolution experiments. Under the tested conditions, the γ-CD-based formulations demonstrated favorable dissolution performance, identifying γ-CD systems as promising alternatives to the β-CD-based carriers evaluated previously. This finding therefore extends the existing literature by considering a previously unexplored CD family in a systematic comparison. However, since HP-β-CD was not included in the PAMPA or *ex vivo* permeation studies, the present data do not establish that γ-CD-based formulations provide superior lipid membrane permeability or intestinal transport compared with HP-β-CD.

However, despite the encouraging findings reported to date, CD-based BSE formulations have not yet been evaluated in clinical studies. Collectively, the available evidence, including the findings of the present study, warrants further translational development and clinical evaluation of this formulation strategy. Importantly, the present *in vitro* and *ex vivo* findings do not establish enhanced systemic exposure or therapeutic efficacy; comparative *in vivo* pharmacokinetic studies are required to determine whether the observed advantages translate into improved oral bioavailability.

Conclusions

This study demonstrates that CD complexation markedly improves the biopharmaceutical performance of BAs. The favorable findings from the γ-CD-based formulations support our initial hypothesis that the more expansive γ-CD cavity may provide an improved structural fit for the investigated guest molecules, while the precise host–guest interactions still need clarification by individual BAs. Lyophilized γ-CD formulations exhibited substantially enhanced dissolution in both fasted- and fed-state biorelevant media, as well as improved permeability, while maintaining higher physical- and chemical stability under accelerated conditions.

Importantly, the results show that formulation performance is determined not simply by solubilization, but by the interplay of solubilization, free fraction, and membrane interactions, enabling a rational formulation optimization strategy. In this context, native γ-CD achieved a more favorable balance, enabling prolonged transmembrane flux and higher permeation, whereas HP-γ-CD, although possessing more solubilizing capacity, demonstrated increased membrane retention and reduced transport efficiency in the *ex vivo* model.

These findings provide the first direct comparative evidence that γ-CD derivatives may surpass the commonly used β-CD systems in terms of boswellic acid dissolution, highlighting the significance of CD selection as a critical factor in formulation success.

Overall, the native γ-CD-based formulation provides a natural, scalable, and pharmaceutically feasible strategy for enhancing boswellic acid delivery. Further *in vivo* pharmacokinetic and efficacy studies are required to determine whether these improvements translate into enhanced intestinal absorption, following any necessary formulation optimization.

Acknowledgements

The authors thank Professor János Madarász (Budapest University of Technology and Economics, Budapest, Hungary) for performing the P-XRD measurements. The donation of CDs used in this study by CycloLab Ltd. (Budapest, Hungary) is gratefully acknowledged. This work was supported by the National Research Development and Innovation Office of Hungary (FK152458 to G.T.B.).

Author contributions

CRediT: **Marcell Stifter-Mursits**: Conceptualization, Formal analysis, Investigation, Methodology, Validation, Visualization, Writing – original draft; **Péter Püski**: Formal analysis, Investigation, Visualization, Writing – original draft; **Vivien Bárdos**: Formal analysis, Investigation, Methodology; **Barbara Ádám**: Formal analysis, Investigation; **Levente Szőcs**: Conceptualization, Methodology, Writing – review & editing; **Dávid Hamar**: Formal analysis, Investigation; **Nikolett Kállai-Szabó**: Methodology, Writing – review & editing; **István Antal**: Methodology, Resources; **Judit Hohmann**: Methodology, Resources, Supervision; **Attila Hunyadi**: Resources, Supervision, Writing – review & editing; **Fang-Rong Chang**: Investigation, Methodology; **Bence Sipos**: Formal analysis, Investigation; **Gábor Katona**: Investigation, Methodology, Writing – review & editing; **Réka Angi**: Conceptualization, Methodology, Supervision, Writing – review & editing; **György T. Balogh**: Funding acquisition, Methodology, Resources, Supervision, Writing – review & editing.

Declaration of generative AI use

During the preparation of this work, the authors used ChatGPT (version GPT-5.4, OpenAI) to assist with language editing, including rephrasing sentences and identifying alternative wording, and to assist with writing scripts for data visualization. All AI-generated suggestions and code were reviewed, edited, and verified by THE AUTHORS. *T*HE AUTHORS take full responsibility for the content of the publication, including the accuracy and integrity of the data, analyses, interpretations, and final manuscript.

Disclosure statement

The authors declare that they have no conflict of interest.

Funding

This study was supported by the Nemzeti Kutatási Fejlesztési és Innovációs Hivatal, FK152458.

Data availability statement

The data that support the findings of this study ares available from the corresponding author upon reasonable request.

References

Abdel-Tawab M, Werz O, Schubert-Zsilavecz M. 2011. *Boswellia serrata*: an overall assessment of in vitro, preclinical, pharmacokinetic and clinical data. Clin Pharmacokinet. 50(6):349–369. https://doi.org/10.2165/11586800-000000000-00000

Al-Harrasi A, Khan AL, Asaf S, Al-Rawahi A. 2019. Biology of genus Boswellia. Springer International Publishing. https://doi.org/10.1007/978-3-030-16725-7

Angi R et al. 2025. Harnessing cyclodextrins for enhanced ocular delivery of carotenoid derivatives: from development to ex vivo characterization. Carbohyd Poly Technol Appl. 9:100718. https://doi.org/10.1016/j.carpta.2025.100718
Avdeef A. 2003. Absorption and drug development: solubility, permeability, and charge state. John Wiley & Sons. https://doi.org/10.1002/047145026X
Bairwa K, Jachak SM. 2015. Development and optimisation of 3-Acetyl-11-keto-β-boswellic acid loaded poly-lactic-co-glycolic acid-nanoparticles with enhanced oral bioavailability and in-vivo anti-inflammatory activity in rats. J Pharm Pharmacol. 67(9):1188–1197. https://doi.org/10.1111/jphp.12420
Cuoco A, Eriksen JB, Luppi B, Brandl M, Bauer-Brandl A. 2023. When interactions between bile salts and cyclodextrin cause a negative food effect: dynamic dissolution/permeation studies with itraconazole (Sporanox®) and biomimetic media. J Pharm Sci. 112(5):1372–1378. https://doi.org/10.1016/j.xphs.2022.12.010
Efferth T, Oesch F. 2022. Anti-inflammatory and anti-cancer activities of frankincense: targets, treatments and toxicities. Semin Cancer Biol. 80:39–57. https://doi.org/10.1016/j.semcancer.2020.01.015
Eriksen JB, Christensen SB, Bauer-Brandl A, Brandl M. 2022. Dissolution/permeation of albendazole in the presence of cyclodextrin and bile salts: a mechanistic in vitro study into factors governing oral bioavailability. J Pharm Sci. 111(6):1667–1673. https://doi.org/10.1016/j.xphs.2021.11.010
European Directorate for the Quality of Medicines & HealthCare. 2023. Indian frankincense (*Olibanum indicum*) (Monograph No. 01/2013:2310). In European pharmacopoeia (113). Council of Europe.
Gerbeth K et al. 2013. In vitro metabolism, permeation, and brain availability of six major boswellic acids from *Boswellia serrata* gum resins. Fitoterapia. 84:99–106. https://doi.org/10.1016/j.fitote.2012.10.009
Hüsch J et al. 2012. Effect of phospholipid-based formulations of *Boswellia serrata* extract on the solubility, permeability, and absorption of the individual boswellic acid constituents present. J Nat Prod. 75(10):1675–1682. https://doi.org/10.1021/np300009w
Hüsch J et al. 2013. Enhanced absorption of boswellic acids by a lecithin delivery form (Phytosome®) of *Boswellia* extract. Fitoterapia. 84:89–98. https://doi.org/10.1016/j.fitote.2012.10.002
Introspective Market Research. 2024. Frankincense extract market expected to reach USD 734.54 million by 2032, growing at a CAGR of 9.2% from 2024-2032. *GlobeNewswire*. [accessed date 2025 March 10]. https://www.globenewswire.com/news-release/2024/11/22/2985939/0/en/Frankincense-Extract-Market-Expected-To-Reach-USD-734-54-Million-by-2032-Growing-at-a-CAGR-of-9-2-From-2024-2032-Introspective-Market-Research.html
Kimmatkar N, Thawani V, Hingorani L, Khiyani R. 2003. Efficacy and tolerability of *Boswellia serrata* extract in treatment of osteoarthritis of knee – A randomized double blind placebo controlled trial. Phytomedicine. 10(1):3–7. https://doi.org/10.1078/094471103321648593
Krüger P et al. 2008. Metabolism of boswellic acids in vitro and in vivo. Drug Metab Dispos. 36(6):1135–1142. https://doi.org/10.1124/dmd.107.018424
Liu M et al. 2013. A boswellic acid-containing extract attenuates hepatic granuloma in C57BL/6 mice infected with *Schistosoma japonicum*. Parasitol Res. 112(3):1105–1111. https://doi.org/10.1007/s00436-012-3237-7
Loftsson T, Brewster ME. 2011. Pharmaceutical applications of cyclodextrins: effects on drug permeation through biological membranes. J Pharm Pharmacol. 63(9):1119–1135. https://doi.org/10.1111/j.2042-7158.2011.01279.x
Loftsson T, Brewster ME. 2012. Cyclodextrins as functional excipients: methods to enhance complexation efficiency. J Pharm Sci. 101(9):3019–3032. https://doi.org/10.1002/jps.23077
Madisch A et al. 2007. *Boswellia serrata* extract for the treatment of collagenous colitis. A double-blind, randomized, placebo-controlled, multicenter trial. Int J Colorectal Dis. 22(12):1445–1451. https://doi.org/10.1007/s00384-007-0364-1
Másson M, Loftsson T, Másson G, Stefánsson E. 1999. Cyclodextrins as permeation enhancers: some theoretical evaluations and in vitro testing. J Control Release. 59(1):107–118. https://doi.org/10.1016/S0168-3659(98)00182-5
Mathias N et al. 2015. Food effect in humans: predicting the risk through in vitro dissolution and in vivo pharmacokinetic models. Aaps J. 17(4):988–998. https://doi.org/10.1208/s12248-015-9759-z
Meins J, Behnam D, Abdel-Tawab M. 2018. Enhanced absorption of boswellic acids by a micellar solubilized delivery form of *Boswellia* extract. Nfs J. 11:12–16. https://doi.org/10.1016/j.nfs.2018.04.001
Mura P. 2015. Analytical techniques for characterization of cyclodextrin complexes in the solid state: a review. J Pharm Biomed Anal. 113:226–238. https://doi.org/10.1016/j.jpba.2015.01.058
Puskás I, Szente L, Szőcs L, Fenyvesi É. 2023. Recent list of cyclodextrin-containing drug products. Period Polytech Chem Eng. 67(1):11–17. https://doi.org/10.3311/PPch.21222
Reising K et al. 2005. Determination of boswellic acids in brain and plasma by high-performance liquid chromatography/tandem mass spectrometry. Anal Chem. 77(20):6640–6645. https://doi.org/10.1021/ac0506478
Rutkowska M, Olszewska MA. 2026. Advances in drug delivery systems for boswellic acids from *Boswellia serrata*: enhancing oral bioavailability and therapeutic efficacy. Int J Mol Sci. 27(10):4420. https://doi.org/10.3390/ijms27104420

Schmiech M et al. 2021. 11-Keto-α-boswellic acid, a novel triterpenoid from *Boswellia* spp. with chemotaxonomic potential and antitumor activity against triple-negative breast cancer cells. Molecules. 26(2):366. https://doi.org/10.3390/molecules26020366

Schmiech M et al. 2024. Single-dose comparative pharmacokinetic/pharmacodynamic study of a micellar formulation versus a native *Boswellia serrata* dry extract in healthy volunteers. Phytomedicine. 132:155863. https://doi.org/10.1016/j.phymed.2024.155863

Schönbeck C, Madsen TL, Peters GH, Holm R, Loftsson T. 2017. Soluble 1:1 complexes and insoluble 3:2 complexes – Understanding the phase-solubility diagram of hydrocortisone and γ-cyclodextrin. Int J Pharm. 531(2):504–511. https://doi.org/10.1016/j.ijpharm.2017.05.024

Sengupta K et al. 2011. Cellular and molecular mechanisms of anti-inflammatory effect of Aflapin: a novel *Boswellia serrata* extract. Mol Cell Biochem. 354(1–2):189–197. https://doi.org/10.1007/s11010-011-0818-1

Sharma T, Jana S. 2020. Investigation of molecular properties that influence the permeability and oral bioavailability of major β-boswellic acids. Eur J Drug Metab Pharmacokinet. 45(2):243–255. https://doi.org/10.1007/s13318-019-00599-z

Siddiqui MZ. 2011. *Boswellia serrata*, a potential anti-inflammatory agent: an overview. Indian J Pharm Sci. 73(3):255–261. https://doi.org/10.4103/0250-474X.93507

Siemoneit U et al. 2009. On the interference of boswellic acids with 5-lipoxygenase: mechanistic studies *in vitro* and pharmacological relevance. Eur J Pharmacol. 606(1-3):246–254. https://doi.org/10.1016/j.ejphar.2009.01.044

Siemoneit U et al. 2011. Inhibition of microsomal prostaglandin E2 synthase-1 as a molecular basis for the anti-inflammatory actions of boswellic acids from frankincense. Br J Pharmacol. 162(1):147–162. https://doi.org/10.1111/j.1476-5381.2010.01020.x

Solanki N et al. 2024. Boswellic acids: a critical appraisal of their therapeutic and nutritional benefits in chronic inflammatory diseases. Endocr Metab Immune Disord Drug Targets. 24(1):116–129. https://doi.org/10.2174/1871530323666230512154634

Sterk V, Büchele B, Simmet T. 2004. Effect of food intake on the bioavailability of boswellic acids from a herbal preparation in healthy volunteers. Planta Med. 70(12):1155–1160. https://doi.org/10.1055/s-2004-835844

Syrovets T et al. 2005. Inhibition of IκB kinase activity by acetyl-boswellic acids promotes apoptosis in androgen-independent PC-3 prostate cancer cells in vitro and in vivo. J Biol Chem. 280(7):6170–6180. https://doi.org/10.1074/jbc.M409477200

Szejtli J. 1988. Cyclodextrin technology. Springer.

Szente L. 1996. Analytical methods for cyclodextrins, cyclodextrin derivatives and cyclodextrin complexes. In: Atwood JL, Davies JED, MacNicol DD, editors, Comprehensive supramolecular chemistry. Vol. 3. Pergamon. p 253–278.

Tambe A, Mokashi P, Pandita N. 2019. Ex vivo intestinal absorption study of boswellic acid, cyclodextrin complexes and poloxamer solid dispersions using everted gut sac technique. J Pharm Biomed Anal. 167:66–73. https://doi.org/10.1016/j.jpba.2018.12.018

Tambe A, Pandita N, Kharkar P, Sahu N. 2018. Encapsulation of boswellic acid with β- and hydroxypropyl-β-cyclodextrin: synthesis, characterization, in vitro drug release and molecular modelling studies. J Mol Struct. 1154:504–510. https://doi.org/10.1016/j.molstruc.2017.10.061

Tambe A, Pandita N. 2018. Enhanced solubility and drug release profile of boswellic acid using a poloxamer-based solid dispersion technique. J Drug Delivery Sci Technol. 44:172–180. https://doi.org/10.1016/j.jddst.2017.11.025

Tausch L et al. 2009. Identification of human cathepsin G as a functional target of boswellic acids from the anti-inflammatory remedy frankincense. J Immunol. 183(5):3433–3442. https://doi.org/10.4049/jimmunol.0803574

Thulin M. 2020. The genus Boswellia (Burseraceae): the frankincense trees. Acta Universitatis Upsaliensis.

United States Pharmacopeia. 2019. Boswellia serrata extract. In USP–NF: dietary supplement monographs. United States Pharmacopeia.

Usapkar P et al. 2024. QbD-guided phospholipid-tagged nanonized boswellic acid naturosomal delivery for effective rheumatoid arthritis treatment. Int J Pharm X. 7:100257. https://doi.org/10.1016/j.ijpx.2024.100257

Wang H et al. 2009. Targeting NF-κB with a natural triterpenoid alleviates skin inflammation in a mouse model of psoriasis. J Immunol. 183(7):4755–4763. https://doi.org/10.4049/jimmunol.0900521